

# Large-scale biometry with interpretable neural network regression on UK Biobank body MRI

Taro Langner, Håkan Ahlström, and Joel Kullberg

**Abstract**—The UK Biobank study has successfully imaged more than 32,000 volunteer participants with neck-to-knee body MRI. Each scan is linked to extensive metadata, providing a comprehensive survey of imaged anatomy and related health states. Despite its potential for research, this vast amount of data presents a challenge to established methods of evaluation, which often rely on manual input. To date, the range of reference values for cardiovascular and metabolic risk factors is therefore incomplete. In this work, neural networks were trained for regression to infer various biological metrics from the neck-to-knee body MRI automatically. The approach requires no manual intervention or ground truth segmentations for training. The examined fields span 64 variables derived from anthropometric measurements, dual-energy X-ray absorptiometry (DXA), atlas-based segmentations, and dedicated liver scans. The standardized framework achieved a close fit to the target values (median  $R^2 > 0.97$ ) in 7-fold cross-validation with the ResNet50. Interpretation of aggregated saliency maps suggests that the network correctly targets specific body regions and limbs, and learned to emulate different modalities. On several body composition metrics, the quality of the predictions is within the range of variability observed between established gold standard techniques.

## I. INTRODUCTION

As part of the UK Biobank study [1] 100,000 volunteer participants are to be examined with magnetic resonance imaging (MRI). Among the scheduled imaging protocols is neck-to-knee body MRI, resulting in volumetric images with separated water and fat signal. These scans contain comprehensive information about the anatomy of each subject and are accompanied by a wide range of other collected metadata, spanning anthropometric measurements, questionnaires, biological samples, health outcomes, and more. Many of these properties also express themselves in the morphology of the human body and could potentially be inferred by image-based biometry. Techniques involving neural networks have been previously proposed for the analysis of brain MRI for detection of premature aging [2], early symptoms of Alzheimers disease [3] and mental disorders [4]. In heart MRI, related approaches were able to perform measurements of volumes and wall thicknesses of the heart [5]. Similarly, analyses of retinal fundus photographs showed that neural networks were able to leverage image features for the prediction of properties including age, gender, smoking status and blood pressure [6].

This study was supported by a research grant from the Swedish Heart-Lung Foundation and the Swedish Research Council (2016-01040).

**Corresponding author: Taro Langner (taro.langner@surgsci.uu.se)**

T Langner is with the Section of Radiology, Department of Surgical Sciences, Uppsala University, Uppsala, Sweden.

J Kullberg and H Ahlström are with the with the Section of Radiology, of Department of Surgical Sciences, Uppsala University, Uppsala, Sweden, and Antaros Medical, BioVenture Hub, Mölndal, Sweden.

Many of these findings were unexpected as the underlying features are often not easily accessible even to human experts. Research in metabolic and cardiovascular disease has led to increased interest in strategies for the automated analysis of body composition [7]. Individualized measurements of fat and muscle compartments in the body have the potential to provide new insight into the development of various medical conditions at greater detail than analyses based on anthropometric measures such as the body mass index (BMI) [8]. The amount of visceral adipose tissue in particular varies substantially between individuals and is directly related to cardiac and metabolic risk [9]. A more fine-grained analysis is of interest in research such as within the UK Biobank study itself [10] but also as a potential tool for disease screening and individualized treatments. Several imaging techniques exist for the measurement of body fat, including CT and dual-energy X-ray absorptiometry (DXA) [11] based on two-dimensional coronal projections. Chemical-shift encoded water-fat MRI acquires separate volumetric water and fat signal images which have the potential to allow for measurements without ionizing radiation, but can be challenging to evaluate. For the delineation of individual adipose tissue depots in these images various methods have been proposed [12]. Automated image analysis with convolutional neural networks for segmentation has been increasingly common for images of this kind [13] [14] as well as for CT images [15] [16], but requires carefully prepared ground truth segmentation images.

In this work, neural networks were trained and evaluated for biometry on the neck-to-knee body MRI scans of the UK Biobank, with main focus on body composition. The proposed approach extends a previously presented method for automated age estimation [17] and performs a regression, so that no ground truth segmentation images or manual corrections are required, and a numerical target label is used instead. The chosen fields instead range from anthropometric measurements to values from dual-energy X-ray absorptiometry (DXA), multi-atlas-based MRI segmentations, dedicated liver scans and various other sources. Our contribution consists in introducing neural network regression on mean intensity projections of the UK Biobank neck-to-knee body MRI as a novel framework for robust, fully automated and interpretable biometry that is no longer restricted to age estimation alone. The optimized and generalized configuration is presented, the quality of its predictions examined with statistical measures and saliency analysis, and evaluated in the context of other established modalities.

## II. METHODS

A fixed convolutional neural network configuration was trained in cross-validation on two-dimensional representations of the neck-to-knee body MRI. For each examined property, the network was evaluated based on the generated predictions as well as saliency maps highlighting relevant patterns in the input images.

### A. Image data

Of the planned 100,000 MRI scans, 32,323 were available at the time of writing. The recruitment was organized by letter from the National Health Service and the vast majority of participants (94%) self-reported their ethnicity as white British in the initial assessment visit. All scans were acquired at three different centers in the United Kingdom in an imaging time of about six minutes with a dual-echo Dixon technique [18] on a Siemens Aera 1.5T device. The scanned area typically covers the body from neck to knee, whereas the arms and other parts of the body that extend laterally are usually not visible or subject to heavy distortion and artifacts [19]. For our experiments those scans that contained water-fat swaps and other artifacts such as excessive noise, unusual positioning and artificial knee replacements were excluded by visual inspection of the projections by one operator, leaving 31,172 images for training. The volumetric scan stations for a given subject were resampled to a resolution of  $2.23 \text{ mm} \times 2.23 \text{ mm} \times 3 \text{ mm}$  and combined into a volume of  $370 \times 224 \times 174$  voxels. This volume was then cropped and compressed into a downsampled, two-dimensional format showing a coronal and sagittal mean intensity projection with a fat and water signal channel. Each subject was accordingly represented by a two-channel image of  $256 \times 256$  pixels, as seen in Fig. 1, stored in 8bit format for easier processing.

### B. Biological metrics

From the thousands of non-imaging properties collected in the UK Biobank study, a subset of 64 fields with relevant biological metrics was chosen. More than half of the chosen fields are results of the DXA scan for body composition [20] [11], comprising fat and lean mass and percentages in the abdomen, trunk, arms and legs. The second largest group of measurements consists of abdominal composition metrics based on multi-atlas-based segmentations performed by the company AMRA Medical [21] [19] [22] on the neck-to-knee body MRI scans. The measurements describe volumes of adipose tissue depots and muscle groups in the abdomen, trunk and thighs. An additional group of fields contains the basic features of age, sex (1 for male, 0 for female), height, and weight. The age was derived from the year (field 34) and month of birth (field 52) as well as the scanning date from DICOM (field 20201), so that it is accurate to about 15 days [17]. The last group consists of miscellaneous fields such as circumferences of the hip and waist, BMI, the liver fat percentage as measured in a dedicated liver MRI [23], the pulse rate on the imaging visit, and the measured grip strength of the right hand, which is often used as an indicator

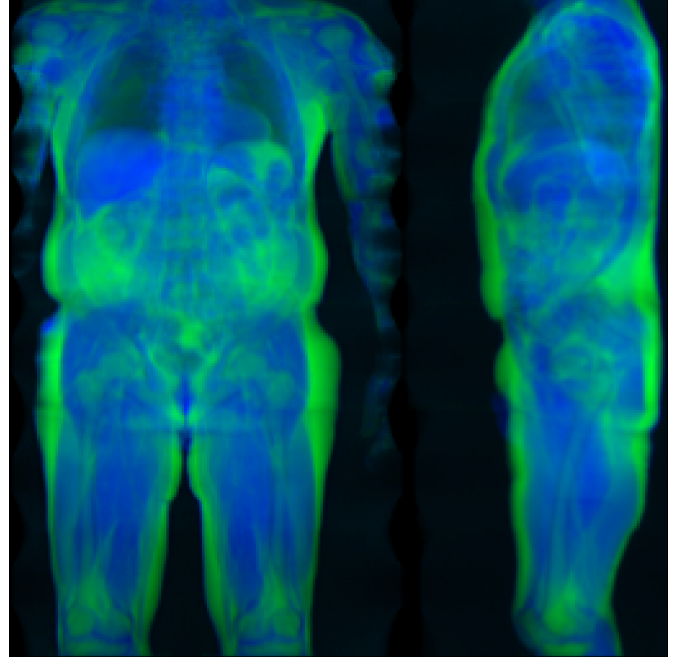


Fig. 1. Two-dimensional format for the volumetric MRI data, which serves as input to the network. The water (blue) and fat (green) signal images are projected along the coronal and sagittal plane and combined as color channels.

in cardiovascular health assessments. Of the 32,323 imaged subjects, only 3,048 have valid entries for all of the chosen fields. These subjects serve as a basis for the saliency analysis. The feature space of the 64 chosen fields for these subjects is visualized in Fig. 2 and showcases some of the underlying patterns relating to sex and body composition. In the following sections, the UK Biobank fields are referred to as reference or ground truth values, together with descriptive names and the unique data field id.

With the aim of using as much training data as possible, networks were trained in 7-fold cross-validation for each field separately, using all subjects with a valid entry that passed quality controls. A master split was generated by random assignment of one of seven labels to each subject, stratified across each group with the same missing values. The 7-fold cross-validation for each field formed a subset of this master split.

### C. Network configuration

For each of the chosen fields a separate convolutional neural network was trained for regression in 7-fold cross-validation. Each unique training sample represents one subject, with the two-dimensional format as extracted from the MRI data as input image and their field entry in the UK Biobank as numerical ground truth target value.

Instead of using a final softmax layer, the activation of a single output neuron of the network was directly translated to the desired measurement. The previously presented regression pipeline [17] for age estimation was optimized in several ways in order to process all of the chosen fields in a viable time frame. The main change consisted in replacing the VGG16 architecture [25] with the more lightweight ResNet50 [26].

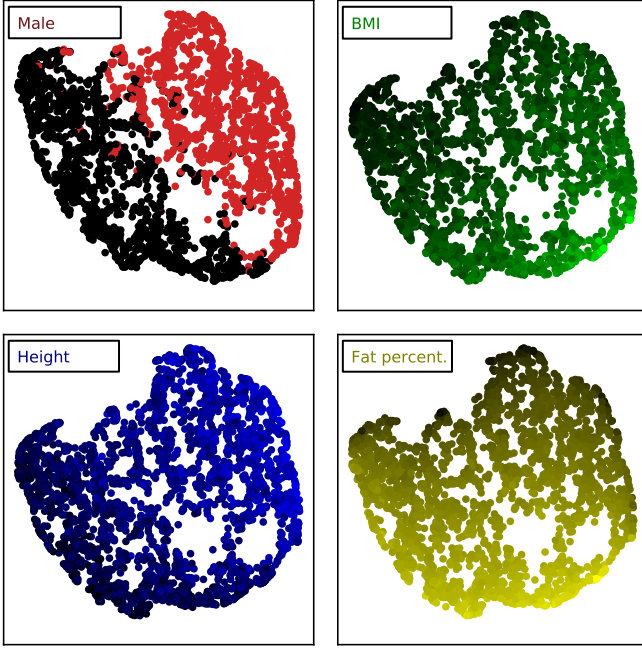


Fig. 2. Feature space of 64 biological metrics for 3,000 subjects. For each subplot, the named variable was removed before dimensionality reduction with UMAP [24] and used for coloring, with brighter intensity for higher values. The sexes (field 31, 0 for females and 1 for males) distinctly divide in two hemispheres whereas the ranges of BMI (field 21001), height (field 12144) and body fat percentage (field 23281) systematically span the opened space.

All numerical target values were standardized by subtracting the mean value and dividing by the standard deviation, as the ResNet50 proved more sensitive to variation in target scaling and shifts. This step resulted in faster convergence and improved stability, so that the total number of iterations could be vastly reduced from 80,000 iterations to just 6,000. To alleviate a tendency of the network to overfit in the final 1,000 iterations, the learning rate of 0.0001 in this phase was reduced by factor ten, typically resulting in a further slight increase in accuracy. Compared to the original configuration, the total training time for a given field was thus reduced by about factor 30, while reaching almost the same accuracy. The original batch size of 32 and augmentation by random translations by up to 16 pixels were retained, with the nearest pixel values being repeated at the borders. All networks were trained on a Nvidia GTX 1080 Ti 11GB graphics card in the framework PyTorch with a mean squared error loss, the optimizer Adam, and parameters pretrained on ImageNet. Each split required about 25 minutes of training time.

These design choices were made based on preliminary results for three representative fields: Age, liver fat (field 22402) and visceral adipose tissue volume (VAT) (field 22407). All presented results were achieved with this exact network configuration<sup>1</sup>, without early stopping or any other attempts to adapt to individual fields for better performance.

#### D. Evaluation

The chosen fields range from volumes to circumferences and simple binary labels, all treated as continuous numerical values. The neural network was trained to predict these values in regression, thereby emulating the reference. When evaluating the inference, the coefficient of determination  $R^2$  is therefore reported to rate the quality of fit, ranging from 1.0 for a perfect fit to negative values where the non-linear network model performs worse than simply estimating the mean. Additionally, the 95% limits of agreement (LoA) as well as the mean absolute error (MAE) are given.

In some cases the network output was thresholded to mimic a classification, with a threshold of 0.5 for prediction of sex and 5.5% for fatty liver disease. Without taking the exclusion criteria into account, the reference liver fat values of 898 of 4219 subjects exceed this threshold. For the prediction, an area under curve (AUC) of the receiver operating characteristic (ROC) curve was calculated.

Several properties were measured redundantly with different modalities. The network performance can accordingly be put into the context of their mutual agreement. We focus on comparing fields derived from atlas-based MRI segmentations [22] to those from DXA [20]. However, both methods examine different regions of interest, leading to systematic differences in their measurements. The MRI-based values were therefore first fit to the DXA values by linear regression before reporting their agreement in this analysis. Similarly, many fields describe features specific to the left and right side of the body. Again, the network performance can be put into the context of this inherent bilateral symmetry, but this analysis is abbreviated to report Pearson's coefficient of correlation  $r$  only.

In addition to statistical measures, salient input features for the network were visualized with guided gradient-weighted class activation maps [27] [28]. The resulting visualizations were combined by co-registration of subjects [29], yielding aggregated saliency maps highlighting those image regions with the highest average effect on the network prediction [17]. Each saliency map was generated by the one network that used the corresponding subject as a validation sample in cross-validation. When visualized, the saliency intensities were squared and overlaid as a heatmap over the water signal image, but no other post-processing was applied.

Some properties could be trivial to predict due to strong correlations with simple non-image features such as age and weight. We therefore also provide the results of multiple linear regression based on the age, sex, height and weight as a baseline for comparison with the neural network performance.

### III. RESULTS

The inferred values closely match the reference in almost all examined fields, and predictions for the field with the median fit ( $R^2 = 0.972$ ) are visualized in Fig. 3<sup>2</sup>. Table I lists the basic fields with a MAE of about 2.5 years for age, 0.8kg for body weight and 1.7cm for height. When thresholded, the classification accuracy for the prediction of sex reached 99.97%, so that only 10 of 31,172 subjects were misclassified.

<sup>1</sup><https://github.com/tarolangner/mri-biometry>

<sup>2</sup>Find detailed plots for all fields in the supplementary material

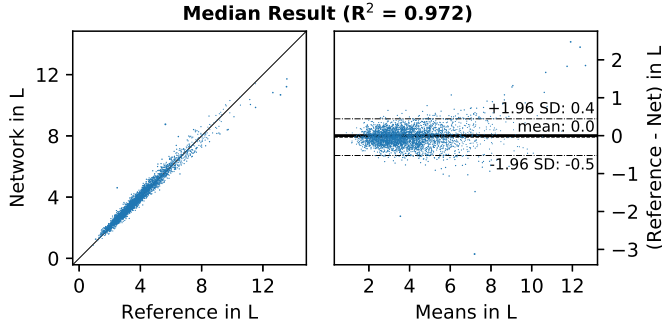


Fig. 3. Visualization of the median result: DXA fat mass of the left leg (field 23266). The diagonal line represents a hypothetical perfect fit, whereas dashed lines represent the 95% limits of agreement (LoA).

Table II gives the main results for DXA<sup>3</sup>, the atlas-based measurements from MRI, and other fields such as liver fat, grip strength, and pulse rate. When thresholded at 5.5% to identify subjects with high liver fat, the predictions reached an accuracy of 90%, with a sensitivity of 73%, specificity of 95% and an AUC-ROC of 0.943. Even though the arms are usually not visible in the images, the network succeeded in estimating the grip strength of the right hand with an MAE of about 5kg and furthermore gave a rough estimate of the pulse rate.

#### A. Saliency analysis

Examples for saliency maps generated by the network are shown in Fig. 4. The saliency indicates that the network on average correctly targets specific structures on the left or right side of the body. Moreover, the estimate of liver fat appears to be mostly based on image areas with actual liver tissue, whereas the prediction of the pulse rate takes into account features of the heart. The BMI appears to be mostly estimated from the knees and lungs, and the grip strength of the right hand is inferred from features of the corresponding side of the upper body.<sup>4</sup>

#### B. Agreement between modalities

Measurements from DXA are compared to those derived from atlas-based segmentations of the MRI in Table III. Each listed comparison yielded lower agreement than achieved by the specific network predictions seen in Tables II and IV. Although only a one-way fitting of MRI to DXA is shown, this analysis was performed in both directions and yielded average LoA between both methods that are on average 70% wider than the LoA between each field and its network predictions.

#### C. Bilateral symmetry

In some cases the accuracy of the network predictions exceeds the bilateral symmetry of the body. For a given property, one limb is accordingly more dissimilar to the opposite limb than to its prediction by the network. A full comparison as

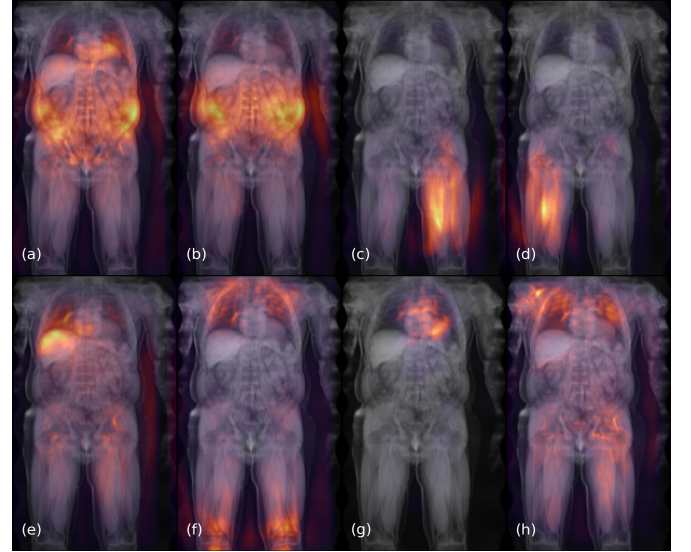


Fig. 4. Aggregated saliency of about 3,000 subjects for: VAT as derived from atlas-based MRI segmentations (field 22407) (a) or DXA (field 23289) (b), muscle volumes of the anterior left (field 22405) (c) and right thigh (field 22403) (d), liver fat (field 22402) (e), BMI (field 21001) (f), pulse rate (field 102) (g) and grip strength (field 47) (h). The network appears to emulate regions of interest used by different modalities and correctly targets specific limbs and organs.

performed for the modalities was not attempted, and only the results of correlation analysis with Pearson  $r$  are reported.<sup>5</sup>

The average bilateral correlation for the anterior and posterior thigh muscle volume amounts to  $r = 0.979$ . The network predictions correlate more strongly with the left- and right-specific measurements for an average  $r = 0.989$ . For DXA, however, the specific prediction accuracy of the network is lower than the bilateral symmetry, with averages of  $r = 0.975$  vs  $r = 0.954$  for the arms and  $0.987$  vs  $0.983$  for the legs. The network was accordingly able to automatically detect bilateral variation and measure the structures within the correct limb for the MRI-based values. Although some individuals show strong unilateral atrophy, this effect is not just due to outliers. The fact that the network learned to specifically target either side of the body is also visible in the saliency maps of Fig. 4 and occurs in both the DXA and MRI-based fields.

## IV. DISCUSSION

The neural network configuration showed robust performance and achieved a close fit to the chosen fields, with a median  $R^2$  above 0.97. It not only learned to accurately estimate volumes and circumferences from the two-dimensional input, but also to emulate different modalities and make measurements specific to either side of the body. The linear regression baseline was outperformed in all cases and indicates that most of these properties can not be trivially deduced from the basic characteristics of age, sex, height, and weight.

When used to infer metrics related to body composition, the network yielded more faithful approximations of the atlas-based measurements from MRI or DXA than obtained by

<sup>3</sup>Find additional DXA Tables IV, V, VI in the supplementary material

<sup>4</sup>Find complete saliency maps for all fields in the supplementary material

<sup>5</sup>Find Table VII in the supplementary material



TABLE I  
INFERENCE OF BASIC FIELDS

field	name	N	unit	[min , max]	mean $\pm$ SD	MAE	LoA	R <sup>2</sup>
/	age	31172	years	[44.6 , 82.3]	63.9 $\pm$ 7.5	2.46	(-5.85 to 6.31)	0.829
31	sex	31172	(male = 1)	[0.0 , 1.0]	0.5 $\pm$ 0.5	0.00	(-0.04 to 0.04)	0.999
12144	height	31172	cm	[140.0 , 204.0]	170.2 $\pm$ 9.4	1.70	(-4.78 to 4.44)	0.938
21002	weight	30382	kg	[39.6 , 169.2]	76.5 $\pm$ 15.1	0.78	(-1.95 to 2.24)	0.995

\*SD: Standard deviation, MAE: Mean absolute error, LoA: Limits of agreement.

TABLE II  
INFERENCE OF MAIN FIELDS

field	name	N	unit	[min , max]	mean $\pm$ SD	MAE	LoA	R <sup>2</sup>	R <sup>2</sup> <sub>lr</sub>
<b>DXA:</b>									
23279	TotalFatFreeMass	4544	kg	[7.5 , 84.3]	49.9 $\pm$ 10.2	0.79	(-2.05 to 1.98)	0.990	0.908
23278	TotalFatMass	4544	kg	[2.7 , 76.1]	26.1 $\pm$ 9.0	0.56	(-1.36 to 1.59)	0.993	0.894
23280	TotalLeanMass	4544	kg	[6.8 , 80.3]	47.3 $\pm$ 9.7	0.82	(-2.07 to 2.11)	0.988	0.904
23281	TotalTissueFat	4544	%	[11.8 , 58.4]	35.2 $\pm$ 8.0	0.67	(-1.67 to 1.68)	0.988	0.740
23282	TotalTissueMass	4544	kg	[9.5 , 154.0]	73.3 $\pm$ 14.5	0.79	(-2.07 to 2.17)	0.994	0.993
23289	VatVolume	4498	L	[0.0 , 6.6]	1.3 $\pm$ 1.0	0.12	(-0.30 to 0.33)	0.972	0.718
<b>MRI:</b>									
22403	AnteriorThighMuscleR	5662	L	[0.6 , 3.7]	1.7 $\pm$ 0.5	0.06	(-0.15 to 0.15)	0.975	0.796
22404	PosteriorThighMuscleR	5662	L	[1.4 , 6.2]	3.4 $\pm$ 0.8	0.08	(-0.21 to 0.21)	0.983	0.829
22405	AnteriorThighMuscleL	5607	L	[0.7 , 3.6]	1.7 $\pm$ 0.5	0.06	(-0.14 to 0.15)	0.975	0.802
22406	PosteriorThighMuscleL	5607	L	[1.3 , 6.3]	3.4 $\pm$ 0.8	0.08	(-0.22 to 0.21)	0.981	0.824
22407	VatVolume	5763	L	[0.1 , 14.4]	3.8 $\pm$ 2.2	0.14	(-0.37 to 0.39)	0.993	0.703
22408	AsatVolume	5763	L	[1.5 , 23.5]	7.1 $\pm$ 3.1	0.22	(-0.62 to 0.61)	0.990	0.822
22409	TotalThighMuscle	5559	L	[4.3 , 19.0]	10.2 $\pm$ 2.5	0.18	(-0.43 to 0.46)	0.992	0.846
22410	TotalTrunkFat	5763	L	[1.9 , 31.6]	10.9 $\pm$ 4.5	0.24	(-0.68 to 0.63)	0.994	0.843
22415	TotalAdiposeTissue	8276	L	[5.5 , 65.9]	21.1 $\pm$ 7.0	0.37	(-0.99 to 1.07)	0.994	0.879
22416	TotalLeanTissue	8276	L	[12.3 , 43.3]	24.2 $\pm$ 4.8	0.64	(-1.92 to 1.69)	0.963	0.846
<b>Other:</b>									
48	waist	30441	cm	[55.0 , 184.0]	88.6 $\pm$ 12.6	3.35	(-8.70 to 8.10)	0.883	0.815
49	hip	30443	cm	[72.0 , 157.0]	101.3 $\pm$ 8.6	2.60	(-6.60 to 6.61)	0.847	0.759
21001	BMI	30124	kg/m <sup>2</sup>	[14.2 , 62.0]	26.6 $\pm$ 4.3	0.41	(-1.13 to 0.99)	0.984	0.969
22402	liverFat	4419	%	[0.0 , 46.0]	4.0 $\pm$ 4.7	1.35	(-4.04 to 4.22)	0.799	0.208
47	gripStrengthRight	30053	kg	[-0.0 , 72.0]	31.3 $\pm$ 10.5	5.08	(-12.92 to 12.87)	0.607	0.583
102	pulseRate	25123	bpm	[33.0 , 157.0]	69.4 $\pm$ 12.1	8.10	(-20.13 to 20.76)	0.262	0.058

\*SD: Standard deviation, MAE: Mean absolute error, LoA: Limits of agreement.

R<sup>2</sup><sub>lr</sub>: Fit of multiple linear regression on age, sex, height and weight.

TABLE III  
AGREEMENT BETWEEN REFERENCE METHODS

property	field <sub>MRI</sub>	field <sub>DXA</sub>	N	term	unit	MAE	LoA	R <sup>2</sup>
VAT	22407	23289	4494	0.42x - 0.3	L	0.17	(-0.45 to 0.45)	0.939
TotalTrunkFat	22410	23284	4538	1.35x + 0.6	kg	0.75	(-1.93 to 1.93)	0.971
TotalFatTissue	22415	23278	4326	1.23x - 0.2	kg	0.85	(-2.30 to 2.30)	0.981
TotalLeanTissue	22416	23280	4326	1.88x + 1.9	kg	1.68	(-4.46 to 4.46)	0.937

\* Transforming measurements from atlas-based MRI segmentations of N subjects to their corresponding values from DXA yields the listed linear regression term, mean absolute error (MAE), and limits of agreement (LoA). In all cases, this agreement is exceeded by the accuracy of their individual network predictions.

substituting these two reference methods for each other. This was still the case even after fitting both reference methods to each other with linear regression. The agreement for both modalities on the UK Biobank reported in previous work [22] yielded similar error bounds, for a sample with considerable overlap to the subjects examined here. The atlas-based method on MRI has also been previously compared to an alternative method based on T1-weighted images [21], yielding LoA for VAT, ASAT and total trunk fat that are on average more than twice as wide as those relative to the network. The variability between these established modalities can largely be accounted for by differing regions of interest. Whereas the atlas-based

method measures VAT up to the thoracic vertebrae Th9 [19], DXA defines VAT as ranging from the top of the iliac crest up to 20% of the distance to the base of the skull [22]. This is reflected in the saliency maps of Fig. 4, indicating that the network correctly learned to emulate the different criteria, based on the numerical target label alone.

Many of the most accurate predictions were made for the atlas-based measurements on MRI, where the accuracy of the network also exceeds the inherent similarity in muscle volumes between the left and right leg. There are several possible explanations for this. In contrast to the DXA-based values, these reference measurements were originally performed on

the same MRI data that served as a basis for the presented method. The lack of outliers in the reference suggests that it closely represents an objective truth that is contained in these images. Furthermore, all images with ground truth values passed the quality control steps applied by the reference. The network was accordingly trained and evaluated on samples that were preselected regarding suitability for body composition analysis. The measurements of the arms and legs from DXA, in contrast, contain outliers and are often based on anatomy that is not entirely contained in the field of view.

There are several key differences between the atlas-based method [19] and the presented approach. The network generates no segmentations for manual refinement or quality control. It furthermore requires hundreds or thousands of labeled ground truth images for training and would likely require retraining for different imaging devices and demographics. The atlas-based method relies on just 31 prototype subjects and has been credited for robustness towards different imaging devices and field strengths. In turn, the network can analyze several scans within just seconds instead of minutes and requires no manual intervention or guidance, so that it can easily be scaled to process tens of thousands of subjects. Even though no segmentations are generated, there is also no restriction on using only segmented images as input, but instead arbitrary numerical target labels can be used. This makes it possible to examine more abstract properties, such as grip strength and pulse rate, and to link them to relevant anatomical regions by saliency analysis.

One limitation of this work consists in the lack of an independent test set. This means that it remains unclear whether the already trained networks would reach similar performance on data from other studies and sources. As the used data has been gathered at three different imaging centers, it at least appears that the protocol can be reproduced sufficiently well at different sites for the UK Biobank study population to allow for robust performance. When applied to data from other studies, such as for example the whole-body MRI scans of the German National Cohort [30], systematic differences in subject demographics, scanning device or protocol are likely to limit the performance however, and retraining of the networks would almost certainly be necessary. The lack of an independent test set might also raise concerns about the network configuration being excessively adapted to the given data. It could be assumed that the repeated runs of the cross-validation during the preliminary experiments may have resulted in design choices that merely represent a coincidental optimum on the cross-validation data itself, with no ability to generalize and possible dependence on confounding factors in the images. However this effect is unlikely to play a significant role since all design choices were based on preliminary experiments on the fields for age, liver fat (field 22402) and VAT (field 22407) only. The resulting configuration is robust without any individual adjustment on thousands of samples for a large variety of fields, so that it is exceedingly unlikely that the high performance is based on simple confounding effects alone.

Many properties could potentially be predicted with greater accuracy by using customized image formats and longer

training times. The resampled, two-dimensional projection of the volumetric scan also retains less than 1% of the original number of values as obtained from MRI, and is furthermore compressed to 8bit. Despite the computational benefits there is no reason to assume that this format is optimal for all of the examined fields.

The distinct water and fat signal as separated by chemical shift likely form a key element in the accurate prediction of those metrics relating to body composition. However, the network has no access to the fat fraction values of the input volume, but instead learns to infer them from the separately normalized fat and water signal projections. The fat fraction can not be easily incorporated in this format, since the projected values are conflated with the background along the projection axis. Future work will consist in exploring more viable ways to incorporate fraction values in the input, which is likely to improve especially the liver fat prediction.

When compared to the previous configuration for age estimation [17], the network for age was trained in cross-validation with about 28% more data. The mean absolute error accordingly decreased as expected, from a previous 2.49 years to 2.46 years, roughly following the previously reported relationship between performance and quantity of training data. The ResNet50 performs similar to the VGG16 when using standardization of the target values, but at far higher speed. Its main disadvantage consists in more diffuse saliency maps, possibly due to the final average pooling layer.

The results show that the presented approach can leverage the two-dimensional image format to estimate not only the age but a wide range of body composition metrics in subjects of the UK Biobank. Given only an abstract, numerical target value and the vast amount of images, the regression network learned to identify the correct body region, tissue or limb as used by the reference methods. In its current form the method could be used to approximate missing values for those subjects who have not yet undergone all of the planned examinations. These estimates could then serve for quality control and as a basis for preliminary analyses. Future work will consist in improving individual measurements with specialized input formats and network configurations, as well as exploring the limits of which other, more abstract properties can be predicted from these scans. Similar approaches could potentially enable the prediction of more variables such as blood biochemistry, disease states and genetic markers.

## V. CONCLUSION

The standardized network configuration robustly predicted properties derived from anthropometric measurements, DXA, atlas-based segmentations, and dedicated liver scans from the neck-to-knee body MR images of the UK Biobank. Saliency and correlation analysis indicate that the network learned to specifically target the left and right side of the body and to emulate different modalities in some of the chosen measurements. Given enough training data for a given demographic and a standardized Dixon imaging protocol, neural networks have the potential to fully automate a wide range of biometry tasks on a single 6-minute neck-to-knee body MRI.

## ACKNOWLEDGMENT

This research has been conducted using the UK Biobank Resource under application no. 14237.

## REFERENCES

- [1] C. Sudlow, J. Gallacher, N. Allen, V. Beral, P. Burton, J. Danesh, P. Downey, P. Elliott, J. Green, M. Landray, B. Liu, P. Matthews, G. Ong, J. Pell, A. Silman, A. Young, T. Sprosen, T. Peakman, and R. Collins, "UK Biobank: An Open Access Resource for Identifying the Causes of a Wide Range of Complex Diseases of Middle and Old Age," *PLOS Medicine*, vol. 12, p. e1001779, Mar. 2015.
- [2] J. H. Cole, R. P. Poudel, D. Tsagkrasoulis, M. W. Caan, C. Steves, T. D. Spector, and G. Montana, "Predicting brain age with deep learning from raw imaging data results in a reliable and heritable biomarker," *NeuroImage*, vol. 163, pp. 115–124, Dec. 2017.
- [3] Y. Ding, J. H. Sohn, M. G. Kawczynski, H. Trivedi, R. Harnish, N. W. Jenkins, D. Lituiev, T. P. Copeland, M. S. Aboian, C. Mari Aparici, *et al.*, "A deep learning model to predict a diagnosis of alzheimer disease by using 18f-fdg pet of the brain," *Radiology*, vol. 290, no. 2, pp. 456–464, 2018.
- [4] S. Shahab, B. H. Mulsant, M. L. Levesque, N. Calarco, A. Nazeri, A. L. Wheeler, G. Foussias, T. K. Rajji, and A. N. Voineskos, "Brain structure, cognition, and brain age in schizophrenia, bipolar disorder, and healthy controls," *Neuropsychopharmacology*, vol. 44, no. 5, p. 898, 2019.
- [5] W. Xue, A. Islam, M. Bhaduri, and S. Li, "Direct multitype cardiac indices estimation via joint representation and regression learning," *IEEE transactions on medical imaging*, vol. 36, no. 10, pp. 2057–2067, 2017.
- [6] R. Poplin, A. V. Varadarajan, K. Blumer, Y. Liu, M. V. McConnell, G. S. Corrado, L. Peng, and D. R. Webster, "Prediction of cardiovascular risk factors from retinal fundus photographs via deep learning," *Nature Biomedical Engineering*, vol. 2, no. 3, p. 158, 2018.
- [7] E. L. Thomas, J. Fitzpatrick, S. Malik, S. D. Taylor-Robinson, and J. D. Bell, "Whole body fat: content and distribution," *Progress in nuclear magnetic resonance spectroscopy*, vol. 73, pp. 56–80, 2013.
- [8] A. M. Prentice and S. A. Jebb, "Beyond body mass index," *Obesity reviews*, vol. 2, no. 3, pp. 141–147, 2001.
- [9] I. J. Neeland, C. R. Ayers, A. K. Rohatgi, A. T. Turer, J. D. Berry, S. R. Das, G. L. Vega, A. Khera, D. K. McGuire, S. M. Grundy, *et al.*, "Associations of visceral and abdominal subcutaneous adipose tissue with markers of cardiac and metabolic risk in obese adults," *Obesity*, vol. 21, no. 9, pp. E439–E447, 2013.
- [10] J. Linge, M. Borgia, J. West, T. Tuthill, M. R. Miller, A. Dumitriu, E. L. Thomas, T. Romu, P. Tunón, J. D. Bell, *et al.*, "Body composition profiling in the uk biobank imaging study," *Obesity*, vol. 26, no. 11, pp. 1785–1795, 2018.
- [11] S. Kaul, M. P. Rothney, D. M. Peters, W. K. Wacker, C. E. Davis, M. D. Shapiro, and D. L. Ergun, "Dual-energy x-ray absorptiometry for quantification of visceral fat," *Obesity*, vol. 20, no. 6, pp. 1313–1318, 2012.
- [12] H. H. Hu, J. Chen, and W. Shen, "Segmentation and quantification of adipose tissue by magnetic resonance imaging," *Magnetic Resonance Materials in Physics, Biology and Medicine*, vol. 29, no. 2, pp. 259–276, 2016.
- [13] S. Estrada, R. Lu, S. Conjeti, X. Orozco-Ruiz, J. Panos-Willuhn, M. M. B. Breteler, and M. Reuter, "Fatsegnet: A fully automated deep learning pipeline for adipose tissue segmentation on abdominal dixon mri," *Magnetic Resonance in Medicine*, vol. 0, no. 0.
- [14] T. Langner, A. Hedström, K. Mörwald, D. Weghuber, A. Forslund, P. Bergsten, H. Ahlström, and J. Kullberg, "Fully convolutional networks for automated segmentation of abdominal adipose tissue depots in multicenter water-fat mri," *Magnetic resonance in medicine*, vol. 81, no. 4, pp. 2736–2745, 2019.
- [15] A. D. Weston, P. Korfiatis, T. L. Kline, K. A. Philbrick, P. Kostandy, T. Sakinis, M. Sugimoto, N. Takahashi, and B. J. Erickson, "Automated abdominal segmentation of ct scans for body composition analysis using deep learning," *Radiology*, vol. 290, no. 3, pp. 669–679, 2018.
- [16] Z. Wang, Y. Meng, F. Weng, Y. Chen, F. Lu, X. Liu, M. Hou, and J. Zhang, "An effective cnn method for fully automated segmenting subcutaneous and visceral adipose tissue on ct scans," *Annals of biomedical engineering*, pp. 1–17, 2019.
- [17] T. Langner, J. Wikstrom, T. Bjerner, H. Ahlstrom, and J. Kullberg, "Identifying morphological indicators of aging with neural networks on large-scale whole-body MRI," *IEEE Transactions on Medical Imaging*, pp. 1–1, 2019.
- [18] H. Hu and H. E. Kan, "Quantitative proton mr techniques for measuring fat," *NMR in biomedicine*, vol. 26, no. 12, pp. 1609–1629, 2013.
- [19] J. West, O. Dahlqvist Leinhard, T. Romu, R. Collins, S. Garratt, J. D. Bell, M. Borgia, and L. Thomas, "Feasibility of MR-Based Body Composition Analysis in Large Scale Population Studies," *PLoS ONE*, vol. 11, Sept. 2016.
- [20] N. Harvey, P. Matthews, R. Collins, C. Cooper, *et al.*, "Osteoporosis epidemiology in uk biobank: a unique opportunity for international researchers," 2013.
- [21] M. Borgia, E. L. Thomas, T. Romu, J. Rosander, J. Fitzpatrick, O. Dahlqvist Leinhard, and J. D. Bell, "Validation of a fast method for quantification of intra-abdominal and subcutaneous adipose tissue for large-scale human studies," *NMR in biomedicine*, vol. 28, no. 12, pp. 1747–1753, 2015.
- [22] M. Borgia, J. West, J. D. Bell, N. C. Harvey, T. Romu, S. B. Heymsfield, and O. D. Leinhard, "Advanced body composition assessment: from body mass index to body composition profiling," *Journal of Investigative Medicine*, vol. 66, no. 5, pp. 1–9, 2018.
- [23] H. R. Wilman, M. Kelly, S. Garratt, P. M. Matthews, M. Milanesi, A. Herlihy, M. Gyngell, S. Neubauer, J. D. Bell, R. Banerjee, *et al.*, "Characterisation of liver fat in the uk biobank cohort," *PloS one*, vol. 12, no. 2, p. e0172921, 2017.
- [24] L. McInnes, J. Healy, and J. Melville, "Umap: Uniform manifold approximation and projection for dimension reduction," *arXiv preprint arXiv:1802.03426*, 2018.
- [25] K. Simonyan and A. Zisserman, "Very Deep Convolutional Networks for Large-Scale Image Recognition," *arXiv:1409.1556 [cs]*, Sept. 2014. arXiv: 1409.1556.
- [26] K. He, X. Zhang, S. Ren, and J. Sun, "Deep Residual Learning for Image Recognition," in *2016 IEEE Conference on Computer Vision and Pattern Recognition (CVPR)*, pp. 770–778, June 2016.
- [27] R. R. Selvaraju, M. Cogswell, A. Das, R. Vedantam, D. Parikh, and D. Batra, "Grad-CAM: Visual Explanations from Deep Networks via Gradient-Based Localization," in *2017 IEEE International Conference on Computer Vision (ICCV)*, (Venice), pp. 618–626, IEEE, Oct. 2017.
- [28] U. Ozbulak, "Pytorch cnn visualizations." <https://github.com/utkuozbulak/pytorch-cnn-visualizations>, 2019.
- [29] S. Ekström, F. Malmberg, H. Ahlström, J. Kullberg, and R. Strand, "Fast Graph-Cut Based Optimization for Practical Dense Deformable Registration of Volume Images," *arXiv:1810.08427 [cs]*, Oct. 2018. arXiv: 1810.08427.
- [30] F. Bamberg, H.-U. Kauczor, S. Weckbach, C. L. Schlett, M. Forsting, S. C. Ladd, K. H. Greiser, M.-A. Weber, J. Schulz-Menger, T. Niendorf, *et al.*, "Whole-body mr imaging in the german national cohort: rationale, design, and technical background," *Radiology*, vol. 277, no. 1, pp. 206–220, 2015.

## VI. SUPPLEMENTARY MATERIAL

TABLE IV  
INFERENCE OF DXA TRUNK FIELDS

field	name	N	unit	[min , max]	mean $\pm$ SD	MAE	LoA	R <sup>2</sup>	R <sup>2</sup> <sub>lr</sub>
<b>Android:</b>									
23244	BoneMass	4544	g	[16.0 , 118.0]	49.0 $\pm$ 13.0	5.62 (-14.28 to 14.80)	0.676		0.411
23245	FatMass	4544	kg	[0.2 , 9.4]	2.5 $\pm$ 1.2	0.11 (-0.30 to 0.32)	0.982		0.835
23246	LeanMass	4544	kg	[0.3 , 6.8]	3.5 $\pm$ 0.8	0.14 (-0.34 to 0.35)	0.945		0.833
23247	TissueFat	4544	%	[8.1 , 65.7]	39.7 $\pm$ 10.5	1.29 (-3.23 to 3.30)	0.975		0.603
23248	TotalMass	4544	kg	[0.5 , 16.4]	6.0 $\pm$ 1.7	0.20 (-0.50 to 0.52)	0.975		0.925
<b>Gynoid:</b>									
23261	BoneMass	4544	g	[53.0 , 516.0]	274.1 $\pm$ 67.1	15.28 (-37.44 to 40.16)	0.912		0.731
23262	FatMass	4544	kg	[0.2 , 13.5]	4.2 $\pm$ 1.5	0.15 (-0.35 to 0.44)	0.980		0.811
23263	LeanMass	4544	kg	[0.4 , 14.1]	7.3 $\pm$ 1.6	0.18 (-0.49 to 0.45)	0.977		0.876
23264	TissueFat	4544	%	[11.8 , 61.5]	36.1 $\pm$ 9.1	0.92 (-2.29 to 2.33)	0.983		0.770
23265	TotalMass	4544	kg	[0.7 , 27.5]	11.8 $\pm$ 2.2	0.22 (-0.58 to 0.65)	0.980		0.915
<b>Trunk:</b>									
23284	FatMass	4544	kg	[1.2 , 46.0]	14.7 $\pm$ 5.9	0.46 (-1.22 to 1.22)	0.989		0.857
23285	LeanMass	4544	kg	[2.4 , 38.6]	22.8 $\pm$ 4.4	0.57 (-1.42 to 1.47)	0.972		0.843
23286	TissueFat	4544	%	[10.5 , 62.1]	38.2 $\pm$ 9.1	0.96 (-2.24 to 2.53)	0.982		0.647
23287	TotalMass	4544	kg	[4.2 , 82.6]	38.3 $\pm$ 8.6	0.71 (-1.75 to 1.94)	0.988		0.957

\*SD: Standard deviation, MAE: Mean absolute error, LoA: Limits of agreement.

R<sup>2</sup><sub>lr</sub>: Fit of multiple linear regression on age, sex, height and weight.

TABLE V  
INFERENCE OF DXA ARM FIELDS

field	name	N	unit	[min , max]	mean $\pm$ SD	MAE	LoA	R <sup>2</sup>	R <sup>2</sup> <sub>lr</sub>
<b>Left arm:</b>									
23249	FatMass	3834	kg	[0.4 , 4.6]	1.3 $\pm$ 0.5	0.12 (-0.34 to 0.35)	0.866		0.747
23250	LeanMass	3834	kg	[1.1 , 5.5]	2.6 $\pm$ 0.8	0.15 (-0.39 to 0.39)	0.936		0.855
23251	TissueFat	3834	%	[11.1 , 60.9]	33.9 $\pm$ 9.8	1.77 (-4.45 to 4.39)	0.947		0.770
23252	TotalMass	3834	kg	[2.0 , 8.3]	4.1 $\pm$ 1.0	0.25 (-0.63 to 0.65)	0.885		0.858
<b>Right arm:</b>									
23253	FatMass	3834	kg	[0.4 , 4.6]	1.4 $\pm$ 0.5	0.12 (-0.35 to 0.33)	0.867		0.744
23254	LeanMass	3834	kg	[1.3 , 5.6]	2.8 $\pm$ 0.8	0.15 (-0.38 to 0.40)	0.940		0.860
23255	TissueFat	3834	%	[11.0 , 60.9]	33.3 $\pm$ 9.6	1.68 (-4.16 to 4.33)	0.949		0.770
23256	TotalMass	3834	kg	[2.2 , 8.3]	4.3 $\pm$ 1.0	0.25 (-0.63 to 0.65)	0.887		0.862
<b>Arms, total:</b>									
23257	FatMass	4544	kg	[0.4 , 9.3]	2.7 $\pm$ 0.9	0.23 (-0.63 to 0.62)	0.885		0.755
23258	LeanMass	4544	kg	[0.9 , 11.0]	5.4 $\pm$ 1.6	0.27 (-0.71 to 0.67)	0.951		0.869
23259	TissueFat	4544	%	[11.1 , 60.9]	33.6 $\pm$ 9.7	1.60 (-3.87 to 4.12)	0.955		0.775
23260	TotalMass	4544	kg	[1.3 , 16.6]	8.4 $\pm$ 1.9	0.44 (-1.10 to 1.18)	0.907		0.876

\*SD: Standard deviation, MAE: Mean absolute error, LoA: Limits of agreement.

R<sup>2</sup><sub>lr</sub>: Fit of multiple linear regression on age, sex, height and weight.



TABLE VI  
INFERENCE OF DXA LEG FIELDS

field	name	N	unit	[min , max]	mean $\pm$ SD	MAE	LoA	R <sup>2</sup>	R <sup>2</sup> <sub>lr</sub>
<b>Left leg:</b>									
23266	FatMass	3834	kg	[0.9 , 13.6]	3.9 $\pm$ 1.5	0.18 (-0.52 to 0.44)	0.972	0.746	
23267	LeanMass	3834	kg	[3.7 , 16.1]	7.9 $\pm$ 1.8	0.29 (-0.68 to 0.81)	0.956	0.879	
23268	TissueFat	3834	%	[10.7 , 62.0]	32.5 $\pm$ 9.5	1.06 (-2.61 to 2.68)	0.980	0.767	
23269	TotalMass	3834	kg	[7.0 , 25.6]	12.3 $\pm$ 2.4	0.38 (-0.97 to 1.07)	0.952	0.871	
<b>Right leg:</b>									
23270	FatMass	3834	kg	[1.0 , 13.5]	3.9 $\pm$ 1.5	0.17 (-0.48 to 0.47)	0.974	0.742	
23271	LeanMass	3834	kg	[4.0 , 15.4]	8.1 $\pm$ 1.9	0.28 (-0.71 to 0.74)	0.960	0.883	
23272	TissueFat	3834	%	[10.7 , 61.9]	32.6 $\pm$ 9.5	1.02 (-2.57 to 2.56)	0.981	0.763	
23273	TotalMass	3834	kg	[6.8 , 25.6]	12.5 $\pm$ 2.4	0.36 (-0.92 to 1.01)	0.957	0.875	
<b>Legs, total:</b>									
23274	FatMass	4544	kg	[1.0 , 27.1]	7.8 $\pm$ 3.0	0.30 (-0.79 to 0.89)	0.979	0.750	
23275	LeanMass	4544	kg	[3.4 , 31.5]	16.0 $\pm$ 3.7	0.48 (-1.14 to 1.33)	0.970	0.888	
23276	TissueFat	4544	%	[10.7 , 62.0]	32.6 $\pm$ 9.5	0.92 (-2.19 to 2.42)	0.985	0.768	
23277	TotalMass	4544	kg	[4.5 , 52.7]	24.8 $\pm$ 4.8	0.63 (-1.81 to 1.53)	0.967	0.880	

\*SD: Standard deviation, MAE: Mean absolute error, LoA: Limits of agreement.

R<sup>2</sup><sub>lr</sub>: Fit of multiple linear regression on age, sex, height and weight.

TABLE VII  
SYMMETRICAL MEASUREMENTS

field <sub>a</sub>	name <sub>a</sub>	field <sub>b</sub>	name <sub>b</sub>	N	r <sub>(a,b)</sub>	r <sub>(a,net)</sub>	r <sub>(b,net)</sub>
22405	MriAnteriorThighLeanMuscleLeft	22403	MriAnteriorThighLeanMuscleRight	5559	0.974	<b>0.988</b>	<b>0.987</b>
22406	MriPosteriorThighLeanMuscleLeft	22404	MriPosteriorThighLeanMuscleRight	5559	0.983	<b>0.991</b>	<b>0.992</b>
23249	DxaArmFatMassLeft	23253	DxaArmFatMassRight	3834	<b>0.971</b>	0.931	0.931
23250	DxaArmLeanMassLeft	23254	DxaArmLeanMassRight	3834	<b>0.978</b>	0.968	0.969
23251	DxaArmTissueFatPercentageLeft	23255	DxaArmTissueFatPercentageRight	3834	<b>0.984</b>	0.973	0.974
23252	DxaArmTotalMassLeft	23256	DxaArmTotalMassRight	3834	<b>0.966</b>	0.941	0.942
23266	DxaLegFatMassLeft	23270	DxaLegFatMassRight	3834	<b>0.989</b>	0.986	0.987
23267	DxaLegLeanMassLeft	23271	DxaLegLeanMassRight	3834	<b>0.984</b>	0.978	0.980
23268	DxaLegTissueFatPercentageLeft	23272	DxaLegTissueFatPercentageRight	3834	<b>0.992</b>	0.990	0.990
23269	DxaLegTotalMassLeft	23273	DxaLegTotalMassRight	3834	<b>0.982</b>	0.976	0.979

\*Correlations between symmetrical fields and network predictions. The fields (a) and (b) correlate by  $r_{(a,b)}$  whereas the network output correlates to field (a) by  $r_{(a,net)}$ . Only those N subjects were evaluated for whom both measurements were available. Bold font denotes numerically higher values.